Analytical and numerical solution to the nonlinear cubic Duffing equation: An application to electrical signal analysis of distribution lines

Analytical and numerical solution to the nonlinear cubic Duffing equation: an application to electrical signal analysis of distribution lines

Roberto Zivieri[1,2]*, Silvano Vergura[1], Mario Carpentieri[1]

[1]*Department of Electrical and Information Engineering, Technical University of Bari, Italy*
[2]*Department of Physics and Earth Sciences and CNISM Unit of Ferrara, University of Ferrara, Italy*

ABSTRACT

The Duffing oscillator represents an important model to describe mathematically the nonlinear behavior of several phenomena occurring in physics and engineering. In this paper, analytical and numerical solutions to the nonlinear cubic Duffing equation governing the time behaviour of an electrical signal are found as a function of the magnitude and of the sign of the nonlinear parameter, of the damping parameter and for different values of the forcing term. A stability analysis of the Duffing equation in the absence of the forcing term is also performed as a function of the sign and magnitude of the nonlinear parameter. A fitting procedure of the Duffing solution to the current signal flowing in different distribution lines allows us to determine the degree of nonlinearity of the electrical signal suggesting a potential way to quantify the nonlinear behaviour of current electrical signals.

Keywords—Duffing equation, Jacobi elliptic functions, elliptic functions, fixed points, electrical signal

*Corresponding author: Roberto Zivieri, roberto.zivieri@unife.it

1. Introduction

The dynamics of nonlinear systems continues to be one of the main issues in the field of engineering [1-6]. On the other hand, a large deal of work has been devoted to the study of nonlinearity of physical systems. In the last decades, the study of nonlinear dynamics has also been one of the topics in several fields of physics especially of condensed matter physics. A large deal of work was done in the field of nonlinear optics, nonlinear hydrodynamics and nonlinear magnetism by looking for exact and numerical solutions of nonlinear differential equations expressed in the form of nonlinear Schroedinger equations describing a plethora of physical systems [7-8].

Great attention has also been given in solid state physics to model atomic interactions by means of anharmonic potentials taking into account the nonlinear interactions occurring in real crystals. This has allowed to describe the dynamics of phonons, quantized excitations around atoms, in simple crystals in terms of anharmonic interactions and to study the surface anharmonicity of simple metals [9].

Among the several models employed in the calculations, the one based on the Duffing oscillator described by the Duffing equation is undoubtedly one of the most famous and successful [10-12]. This equation dates back, for instance, to applications in mechanics, theory of sound and, more generally, in acoustic and has allowed to describe quantitatively the nonlinear effects typical of real dynamical systems.

Since the introduction of the Duffing equation, there has been a lot of work done on this equation. The most important efforts were made to develop analytical and numerical solution methods. Recently, some mathematical methods to solve the Duffing equation have been proposed. In particular, the solution of the cubic-quintic Duffing oscillator including also a strong fifth-power nonlinear term based on the use of trial Jacobi elliptic functions and for both damped and undamped cases [13-14] has been found for an application to a large variety of real systems. For instance, the solution of the Duffing oscillator has been found for reproducing free vibrations of a restrained uniform beam with intermediate lamped mass and the nonlinear dynamics of slender elastic. In

addition, also a) a formalism based on the Laplace decomposition algorithm; b) a procedure consisting of a variational iteration method able to numerically solve the full non-homogeneous cubic Duffing equation; c) a method based on the Newton-harmonic balancing approach to determine numerical solutions to nonlinear cubic-quintic Duffing oscillators; d) a procedure showing that the second-order nonlinear damping oscillator can be reduced to an equation of the normal Abel form; e) an approach based on the modified differential transform method and on the fourth-order Runge-Kutta numerical solution to solve non-linear Duffing equation and f) a method based on the exact solutions of a generalized autonomous Duffing-type equation were developed [15-20]. Some of the above mentioned methods were employed to investigate the dynamical behaviour of a large variety of physical systems that are described by the various forms of the homogeneous Duffing equation.

Indeed, this equation exhibits an enormous range of well-known behaviours in nonlinear dynamical systems and it is widely used. Since the 1970s, it has been largely used in the field of applied mathematics, especially for the study of chaos in systems governed by a nonlinear behaviour [21-25]. Actually, it can be considered one of the simplest equations that describes the chaotic behaviour of a system and gives insights into the dynamical parameters involved.

Recently, an important electrical engineering application of the Duffing oscillator was also proposed consisting of an islanding detection method in Distributed Generation (DG) systems [26]. The term islanding refers to a condition according to which a distributed generator continues to supply power to local loads after it is separated from the rest of the system. This was done to investigate the transformation of the Duffing oscillator from chaotic state to great periodic one and the performance of the suggested method was confirmed by simulations. Moreover, in the same field a study for detecting and for estimating weak signals by means of the Duffing oscillator has been performed [27].

However, to the best of our knowledge, there are not yet direct mathematical applications of the Duffing oscillator in the field of electrical engineering with special emphasis to the analysis of the

behaviour of electrical signals according to the solution to the full and non-homogeneous Duffing equation.

Therefore, the aim of this paper is to show that the cubic Duffing equation describes the time behaviour of an electrical signal. This analysis is supported by a theoretical framework based on the analytical and numerical solution to the homogeneous and non-homogeneous cubic Duffing equation. In particular, the homogeneous cubic Duffing equation is solved analytically under the assumption of negligible damping and the numerical solution is found and discussed in detail both in the homogeneous and non-homogeneous case. Several cases are generally described as a function of the dynamical parameters like the damping term, the forcing term and the nonlinear parameter.

By considering the current flowing in the distribution lines (DLs) of a smart grid (SG) as the processed electrical signal, the deviation of the measured current intensity $i(t)$ from a linear behaviour is also discussed via a fitting procedure of the cubic Duffing numerical solution to the measured data. According to this fitting procedure the value of the nonlinear parameter associated to the cubic term is determined for the different distribution lines. Indeed, it has been found that, for reproducing the time behaviour of the measured $i(t)$, the inclusion of the quadratic and quintic terms in the Duffing equation leads to negligible changes of the calculated electrical signal time behaviour confirming that the main term governing the dynamics is the cubic term.

2. Theoretical Framework

In this section, we present the theoretical framework by studying the time dependence of an electrical signal. In the specific case it is represented by the current $i(t)$ flowing in a power grid. In order to do that, we solve the Duffing equation for studying the dynamical properties of mechanical and electrical systems. The Duffing equation describes the dynamics of a system in the anharmonic regime. This means that, according to it, the deviation from a purely linear regime by means of a nonlinear term weighted by a nonlinear parameter is taken into account. The non-linearity is

responsible for the anharmonic behaviour of the system up to the third order that is another way of expressing the deviation from periodicity typical of harmonic and ideal electrical systems.

Moreover, also a forcing term is included and is characterized by an amplitude and an angular frequency. The analysis is done by choosing the nonlinear parameter either as positive or negative reproducing the case either of a hard or of a soft "spring". The effect of the forcing term on the form of the electrical signal is also investigated.

2.1. Duffing equation: analytical solution for an undamped and unforced system

In this subsection, we discuss an analytical solution to the Duffing equation. To introduce it, we recall the equation governing the dynamics of a series RLC circuit involving the current. It is well known from the circuit theory that in a series RLC circuit the current $i(t)$ is a solution of a second-order non-homogeneous ordinary differential equation expressed in the form [28]

$$\frac{d^2 i(t)}{dt^2} + 2\eta \frac{di(t)}{dt} + \omega_0^2 i(t) = \frac{1}{L}\frac{dv(t)}{dt} \tag{1}$$

where $\eta = \frac{R}{2L}$ (R is the resistance and L is the inductance) is the neper or attenuation angular frequency, $\omega_0 = \frac{1}{(LC)^{1/2}}$ is the resonance frequency (C is the capacitance) and $v(t) = V_0 \sin(\omega t)$ is the time varying voltage generator with V_0 the maximum value of the voltage and ω the angular frequency of the forcing term. Straightforwardly, the well-known analytical solution to Eq.(1) can be expressed as the sum of a combination of either real or complex exponential functions (depending on the ratio between the attenuation and the resonance frequency) and of a particular solution of the complete equation.

In real systems, there is a deviation towards a non-linear behaviour, so that Eq.(1) does not describe the real trend of the current flowing in the RLC circuit. Starting from the well-known Eq.(1) and by including the cubic nonlinear term, it is possible to write the corresponding Duffing equation. For the sake of simplicity, we express all the terms appearing in Eq.(1) in dimensionless

units where the dimensional current $i(t)$ is replaced by a generic variable $y(\tau)$ with τ the dimensionless time. The dimensionless nonlinear second-order ordinary Duffing equation can be written in the form:

$$\ddot{y}(\tau)+\gamma\dot{y}(\tau)+\varepsilon y^3(\tau)+y(\tau)=\alpha\cos(\tilde{\omega}\tau) \tag{2}$$

where the symbol "." denotes the time derivative with respect to τ. Here, $y=\frac{i}{I_{\max}}$ is dimensionless with $I_{\max}$ the maximum current intensity, $\tau=\frac{t}{T}$ with T the period, $\gamma=\frac{R/L}{\omega_0}=R\sqrt{\frac{C}{L}}$ is the dimensionless damping coefficient , $\tilde{\omega}=\frac{\omega}{\omega_0}$, ε is the non-linear parameter governing the non-linear behaviour (cubic term), $\alpha=\frac{V_0\omega}{L}\frac{1}{I_{\max}}\frac{1}{\omega_0^2}$ is the maximum value of the amplitude of the forcing term in dimensionless units. For $\varepsilon > 0$ the dynamics is equivalent to that of a "hard spring", while for $\varepsilon < 0$ we deal with a "soft spring" dynamics.

We now give an exact analytical solution to Eq.(2) in the absence of damping ($\gamma = 0$) and in the unforced case ($\alpha = 0$). This condition, although not usual, corresponds to power systems where the damping effects can be considered negligible and to the free regime of the generators when, for example, a temporary breakdown of the electrical line takes place. The analytical solution is found as a function of the nonlinear parameter. In this special case, the solution to Eq.(2) takes the form:

$$y_{\pm}(\tau)=B\ \mathrm{sn}\left[\pm j\frac{\sqrt{2}}{2}\left(\left(-1+\left(1+2\varepsilon y_1\right)^{1/2}\right)\left(\tau+y_2\right)^2\right)^{1/2}\Big|\frac{1+\left(1+2\varepsilon y_1\right)^{1/2}}{1-\left(1+2\varepsilon y_1\right)^{1/2}}\right] \tag{3}$$

where the subscripts ± denote the two solutions (one positive and one negative), j is the imaginary unit and the constant B on the second member is $B=-j\left(\frac{2y_1}{-1+\left(1+2\varepsilon y_1\right)^{1/2}}\right)^{1/2}$, $m=\frac{1+\left(1+2\varepsilon y_1\right)^{1/2}}{1-\left(1+2\varepsilon y_1\right)^{1/2}}$ is the parameter expressed by a real number, $y_-(\tau)=-y_+(\tau)$ and y_1 and y_2 are integration constants. The

symbol “sn” stands for Jacobian elliptic function sn ($j\,u|\,m$) defined in the complex plane where in the present case $u=\pm\frac{\sqrt{2}}{2}\left(\left(-1+\left(1+2\varepsilon y_1\right)^{1/2}\right)\left(\tau+y_2\right)^2\right)^{1/2}$. In Eq.(3) the elliptic function sn ($j\,u|\,m$) is a doubly periodic meromorphic function with real quarter-period $K = u(\varphi= \pi/2)$ and imaginary quarter-period $jK'=j\,u\left(m_1,\varphi=\pi/2\right)$ where $m_1 = 1\text{-}m$ is the complementary parameter still expressed by a real number. In Eq.(3) all terms depend on ε and u is a function of both the integration constants y_1 and y_2.

By using Jacobi’s imaginary transformation according to which sn ($j\,u|\,m$) = j sc ($u|\,m_1$), Eq.(3) can be rewritten in the final form in terms of the elliptic function sc($u|\,m_1$), viz:

$$y_{\pm}(\tau)=B_1\ \mathrm{sc}\left[\pm\frac{\sqrt{2}}{2}\left(\left(-1+\left(1+2\varepsilon y_1\right)^{1/2}\right)\left(\tau+y_2\right)^2\right)^{1/2}\Big|-\frac{2\left(1+2\varepsilon y_1\right)^{1/2}}{1-\left(1+2\varepsilon y_1\right)^{1/2}}\right] \tag{4}$$

where $B_1=\left(\frac{2y_1}{-1+\left(1+2\varepsilon y_1\right)^{1/2}}\right)^{1/2}$ and sc($u|\,m_1$) with $m_1=-\frac{2\left(1+2\varepsilon y_1\right)^{1/2}}{1-\left(1+2\varepsilon y_1\right)^{1/2}}$. In Eq.(3) and (4) the first argument $u=\pm\frac{\sqrt{2}}{2}\left(\left(-1+\left(1+2\varepsilon y_1\right)^{1/2}\right)\left(\tau+y_2\right)^2\right)^{1/2}$ is generically expressed by the following integral:

$$u(\varphi,m)=\int_0^{\varphi}\frac{d\theta}{\left(1-m\sin^2\theta\right)^{1/2}} \tag{5}$$

and the angle φ=am (u, m) = am (u) is called the Jacobi amplitude of the argument u, where the script “am” stands for the abbreviation of amplitude and such that sn(u)=sin(φ). The solution expressed by Eqs.(3) and (4) for $\varepsilon\to 0$ tends to the well-known one of the harmonic oscillator in terms of transcendental circular functions. A numerical discussion of the above mentioned solution as a function of the nonlinear parameter ε is performed in Sect. 2.2. The numerical solution to the complete Duffing equation as a function of the nonlinear parameter and of the forcing term is discussed in Sect. 2.3.

2.2. Dependence on the nonlinear parameter of the analytical solution for $\gamma=0$ and $\alpha=0$

In this subsection, a numerical study of the effect of non-linearity on the analytical solution to the Duffing equation expressed in Eq.(2) is performed. This is accomplished by studying the dependence of the $y(\tau)$ on the parameter ε. The exact solution to the Duffing equation ($y_+(\tau)$ in Eq.(4)) is shown in Fig.1 as a function of ε. In the numerical calculation we have taken $y_1 = 1$ and $y_2 = 1$ which determine the initial values. From a numerical check, it was found that the shape of the solution does not essentially depend on the values of the integration constants but the number of oscillations varies by changing the values of y_1 and y_2. The effect of the increase of the nonlinear parameter is a reduction of the amplitude and at the same time an increase of the oscillation frequency resulting in a narrowing of the wave. In this case, the deformation of the wave profile is not so accentuated. Therefore, the general effect of non-linearity is to modulate the amplitude and frequency behaviour. Moreover, the oscillation is highly nonlinear especially for large values of ε as indicated by the deformed wave-profile with pointed crests and troughs especially in panels Fig.1(e-f).

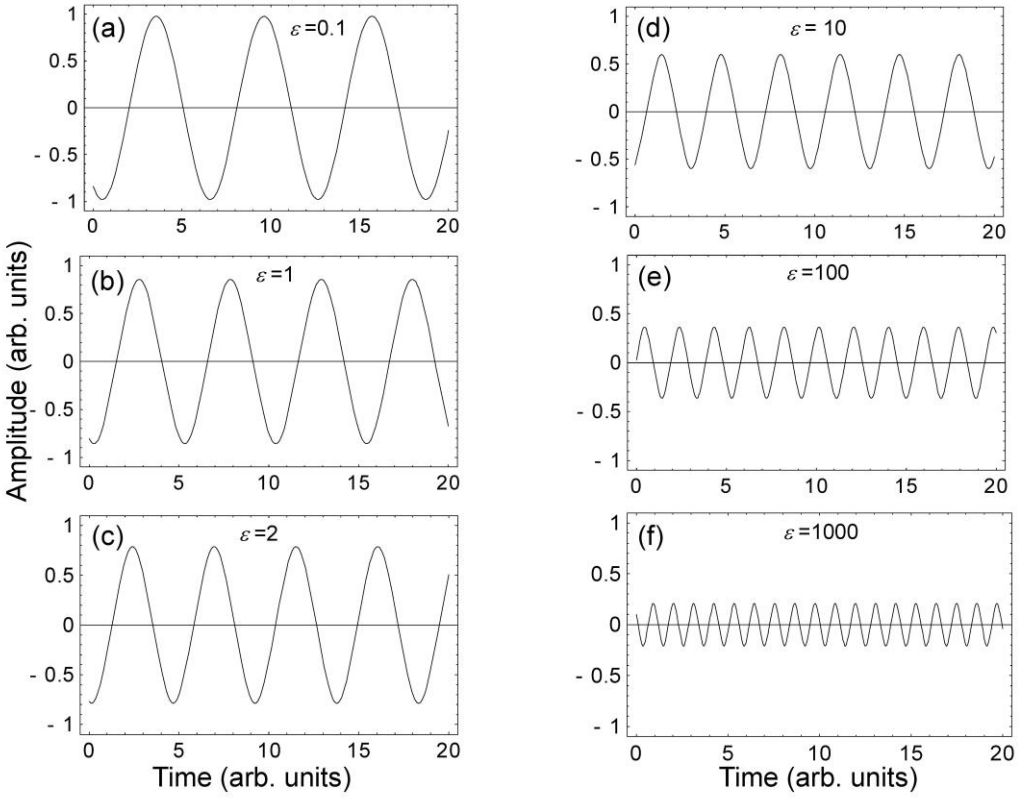

Fig. 1. Analytical solution to the Duffing equation as a function of time for different values of the nonlinear parameter and for $\gamma = 0$ and $\alpha = 0$. (a): $\varepsilon = 0.1$. (b): $\varepsilon = 1$. (c): $\varepsilon = 2$. (d): $\varepsilon = 10$. (e): $\varepsilon = 100$. (f): $\varepsilon = 1000$.

2.3. Numerical solution to the Duffing equation: dependence on the nonlinear parameter and forcing term

In this subsection, we discuss the time behaviour of $y(\tau)$ by solving numerically the Duffing equation. The numerical integration of the nonlinear differential equation (Eq.(2)) has been performed by using a Mathematica routine that determines the function $y(\tau)$ as an interpolating function object for given values of τ providing approximated values of y over the range of τ values considered. The solution is found iteratively starting from a particular value of τ also outside the range considered (in the present case it was chosen $\tau = 0$) which expresses the initial conditions $y(0)$ and $\dot{y}(0)$ and taking a sequence of steps which eventually cover the whole range of τ. First, we

consider the Duffing equation solution by setting $\alpha = 0$ in Eq.(2), namely in the absence of the forcing term that would correspond to the condition of free generators. In all the following calculations on the solution to the Duffing equation the damping coefficient is fixed at $\gamma = 0.5$ that corresponds to a realistic value within the under-damped regime $0 \leq \gamma < 2$. Other choices in the same range would lead to qualitatively similar results.

The trend of the time-domain signal $y(\tau)$ is displayed in Fig.2 for different values of the nonlinear parameter. The general effect is a reduction of the signal amplitude with increasing ε. In addition, there is a frequency modulation especially for large values of ε also connected to the raising of nonlinear effects. This is shown by the narrowing of the signal profile in correspondence of crests and troughs. However, this modulation effect is accentuated with respect to the one found when $\gamma = 0$ (see Fig.1). This means that the damping reinforces the frequency modulation mainly due to the nonlinear term.

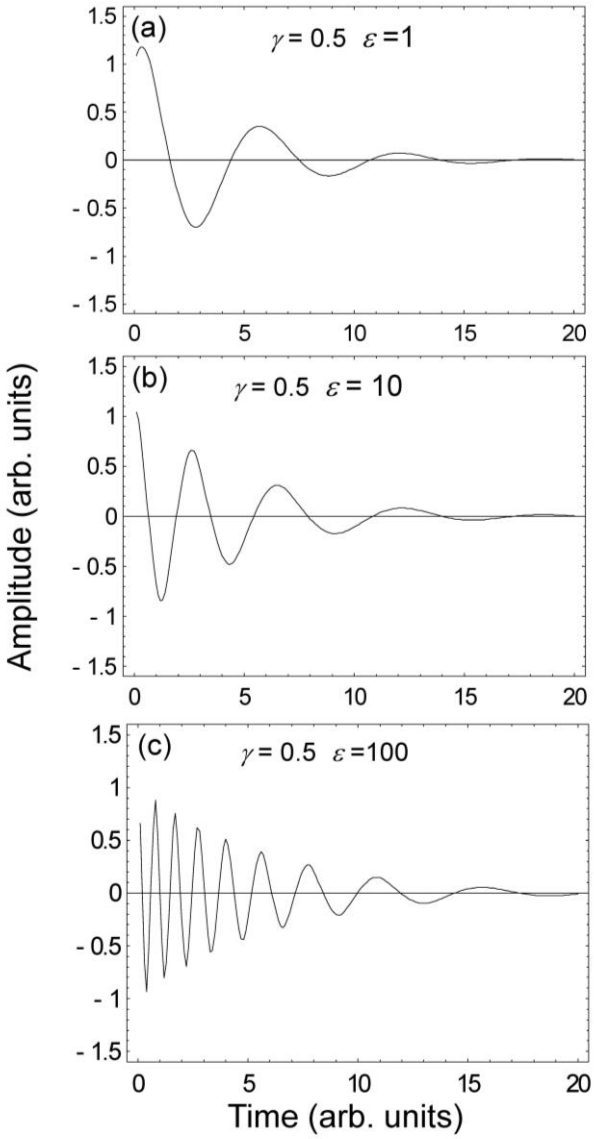

Fig. 2. Solution to the Duffing equation at fixed damping coefficient γ = 0.5 and with no forcing term (α = 0) for different values of the nonlinear parameter. (a): ε = 1. (b): ε = 10. (c): ε = 100.

Interestingly, the Duffing equation numerical solution including also the effect of the sinusoidal forcing term gives further insights for understanding the real behaviour of an electrical signal. The results of this analysis are shown in Fig.3. In Fig.3(a-c) for a forcing coefficient α=1 and for a forcing angular frequency $\tilde{\omega} = 1$ it is evident a deviation from a purely periodical behaviour with increasing ε, which in turn gives rise to the nonlinear behaviour. The amplitude modulation mainly due to the damping effect is almost entirely masked by the effect of the forcing, while the frequency modulation is evident especially for ε = 100 for the first instants of time. Fig.3(d-f) show the

corresponding results obtained for α = 10. Interestingly, at larger forcing the frequency modulation is less accentuated even at ε = 100. Again, nonlinearity effects are present and can be traced into the doubling of the crests and troughs. Indeed, at fixed α the increase of ε by one order of magnitude (see Fig.3(e)) induces a reduction of the amplitude.

Fig.4 illustrates the numerical results for the electrical signal by varying the angular frequency of the forcing term for fixed ε=1 and for two different values of the forcing term, α = 1 (Fig.4(a-c)) and α = 10 (Fig.4(d-f)). The effect of increasing $\tilde{\omega}$ is equivalent to that of a damping. Indeed, it is evident the amplitude modulation passing from $\tilde{\omega}=1$ to $\tilde{\omega}=10$.

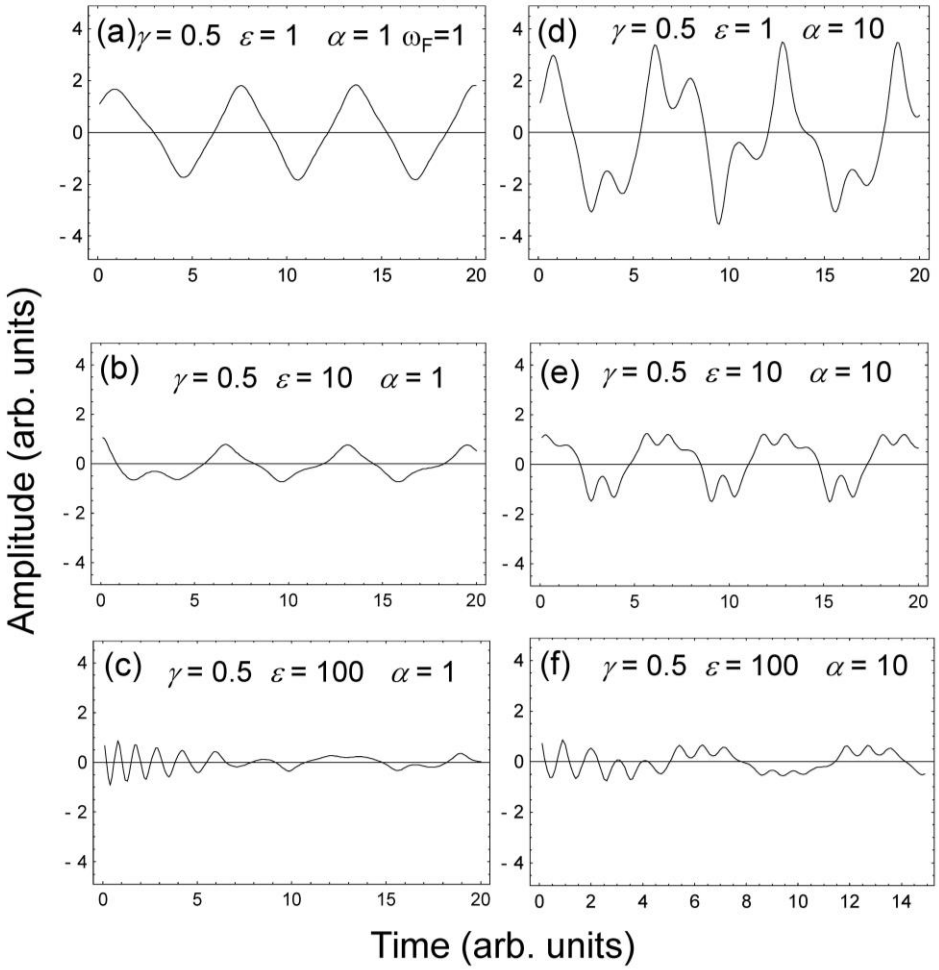

Fig. 3. Solution to the Duffing equation at fixed damping coefficient γ = 0.5 for different values of the forcing term and of the nonlinear parameter. (a): ε = 1, α =1. (b): ε = 10, α =1. (c): ε = 100, α =1. (d): ε = 1, α =10. (e): ε = 10, α =10. (f): ε = 100, α =10. In all case the angular frequency of the forcing term is $\tilde{\omega}=1$.

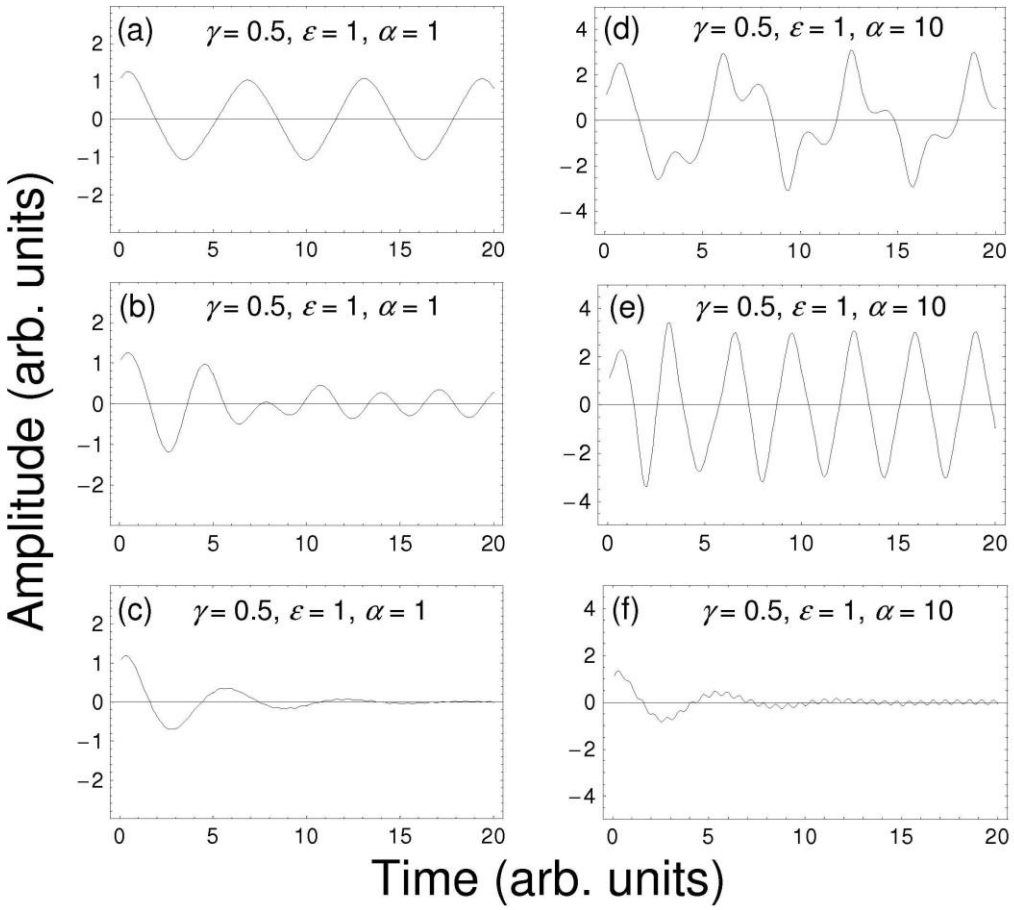

Fig. 4. Solution to the Duffing equation at fixed damping coefficient γ = 0.5, fixed positive nonlinear parameter ε = 1, two different values of the forcing term α as a function of the forcing frequency $\tilde{\omega}$. (a): $\tilde{\omega}=1$ and forcing term α = 1. (b): $\tilde{\omega}=2$ and forcing term α = 1. (c): $\tilde{\omega}=10$ and forcing term α = 1. (d): $\tilde{\omega}=1$ and forcing term α = 10. (e): $\tilde{\omega}=2$ and forcing term α = 10. (f): $\tilde{\omega}=10$ and forcing term α = 10.

On the other hand, the frequency modulation, especially evident for $\tilde{\omega}=2$, is masked by the amplitude modulation at larger angular frequencies ($\tilde{\omega}=10$), namely the amplitude modulation strongly prevails. A larger amplitude of the forcing term (α = 10) produces strong changes in the electrical signal especially by determining a strong frequency modulation that was less evident for α=1. The same attenuation effect that plays the role of a damping is present for $\tilde{\omega}=10$. To summarize, the main effect is a change of the shape of the electrical signal, but no consistent

modifications are present in terms of modulation.

To complete the analysis it has been also numerically studied the effect of a negative nonlinear parameter on the time behaviour of an electrical signal. The negative value of ε describes an active nonlinear component. The results of this analysis are shown in Fig.5 for fixed amplitude and angular frequency of the forcing term $\alpha = 1$ and $\tilde{\omega} = 1$, respectively.

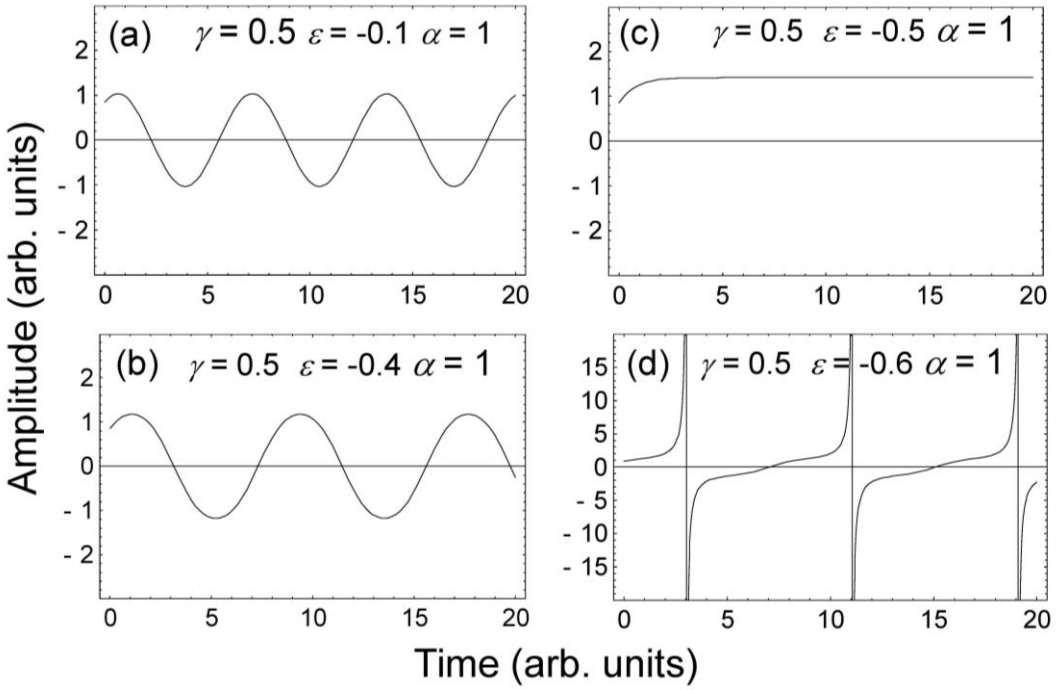

Fig. 5. Solution to the Duffing equation at fixed damping coefficient $\gamma = 0.5$ and $\alpha = 1$ as a function of the negative nonlinear parameter. (a): $\varepsilon = -0.1$. (b): $\varepsilon = -0.4$. (c): $\varepsilon = -0.5$. (d): $\varepsilon = -0.6$.

There is a drastic change of the signal profile with increasing the negative value of the nonlinear parameter. At $\varepsilon = -0.1$ the electrical signal is still almost periodic and the profile is very similar to that of a harmonic wave, but at $\varepsilon = -0.5$ there is a change towards a completely different profile corresponding to that of a localized wave in the form of a hyperbolic transcendental function. At $\varepsilon = -0.6$ the wave amplitude becomes infinite at periodic instant of times. This quick variation in the range [-0.6 ÷ -0.4] and especially the divergence for $\varepsilon = -0.6$ is due to the cubic power of the nonlinear term. Finally, we have found that the inclusion of either an additional quadratic term in

the Duffing equation (Eq.(2)) proportional to $y(\tau)\,|\,y(\tau)\,|$ or of a quintic term proportional to $y^5(\tau)$ does not essentially change the above described results in terms of non-linear behaviour, which are mainly affected by the cubic term.

3. Stability Diagram And Fixed Points

In this section, we discuss the stability of the Duffing equation in the absence of a forcing term as a function of the parameter ε in order to investigate the effect of the non-linearity on the stability diagram and on the fixed points. In principle, the fixed points should be studied by starting from the complete equation in the presence of the forcing term on the second member of Eq.(2). However, a simple argument allows us to exclude this case from the stability discussion. Indeed, when the forcing is taken into account, strictly speaking there would not be any fixed points due to their time dependence related to the forcing term. The stability analysis is performed for ε >0. The stability diagram is studied by discussing also the fixed points for the negative sign in the linear term of Eq.(2) for α = 0. This would correspond to the rather unusual case of a negative capacitance [29].

In its general form, Eq.(2) written for α = 0 can be expressed as the following system of first-order differential equations (by omitting, for the sake of simplicity, the time dependence):

$$\begin{cases} \dot{x} = \mp y - \varepsilon y^3 - \gamma x \\ \dot{y} = x \end{cases} \tag{6}$$

where the minus (plus) sign of the first term on the right member of the first equation is related to the positive (negative) sign of the linear term. The fixed points of Eq.(6) are found from $\dot{y}(t) = x(t) = 0$, so that:

$$\dot{x} = \mp y - \varepsilon y^3 \tag{7}$$

For the positive sign of the linear term, the solution to Eq.(7) yields $F_1 = \left(\frac{j}{\sqrt{\varepsilon}}, 0\right)$, $F_2 = (0,0)$ and $F_3 = \left(-\frac{j}{\sqrt{\varepsilon}}, 0\right)$. Apart from the trivial fixed point in the origin of the stability diagram, there are no fixed

points in the real domain and this would correspond to an absence of fixed periods of the oscillation.

We now analyze the stability diagram in the case of the negative sign in the linear term. The solution to Eq.(7) gives the three fixed points in the stability diagram: $F_1 = \left(-\frac{1}{\sqrt{\varepsilon}},0\right)$, $F_2 = (0,0)$ and $F_3 = \left(+\frac{1}{\sqrt{\varepsilon}},0\right)$. The fixed points are independent of the magnitude of the value of γ, lie on the *x*-axis and would merge asymptotically towards the origin for strong nonlinearity condition, that is for large values of ε. The analysis of the stability of F_1, F_2 and F_3 can be performed by differentiating Eq.(6) and considering the positive sign. We get two second-order differential equations, which can be written in matrix form as:

$$\begin{bmatrix} \ddot{x} \\ \ddot{y} \end{bmatrix} = \begin{bmatrix} -\gamma & 1-3\varepsilon y^2 \\ 1 & 0 \end{bmatrix} \begin{bmatrix} \dot{x} \\ \dot{y} \end{bmatrix} \tag{8}$$

The solution of the eigenvalue problem leads to:

$$\lambda_{\pm}^{F_2} = \frac{1}{2}\left(-\gamma \pm \left(\gamma^2+4\right)^{1/2}\right)$$
$$\lambda_{\pm}^{F_1,F_3} = \frac{1}{2}\left(-\gamma \pm \left(\frac{\gamma^2\varepsilon + 4\varepsilon - 12}{\varepsilon}\right)^{1/2}\right). \tag{9}$$

For any value of $\gamma \geq 0$ there is always a real and positive root $\lambda_{+}^{F_2} > 0$. Hence, the fixed point F_2 is always unstable and, as expected, its stability condition is not a function of ε. By contrast, the stability condition of F_1 and F_3 fixed points strictly depends on the value of ε. Let's discuss first the nature and the sign of the $\lambda_{\pm}^{F_1,F_3}$ eigenvalues for $\gamma > 0$. It turns out that $\lambda_{\pm}^{F_1,F_3}$ are real and negative for $0 < \varepsilon < 3$ and for $\gamma > \left(\frac{12-4\varepsilon}{\varepsilon}\right)^{1/2}$. Instead, they are complex for $0 < \varepsilon < 3$ and for $0 < \gamma < \left(\frac{12-4\varepsilon}{\varepsilon}\right)^{1/2}$ with $\mathrm{Re}[\lambda_{\pm}^{F_1,F_3}] < 0$. Hence, for $0 < \varepsilon < 3$, F_1 and F_3 are asymptotically stable. On the other hand, for $\gamma = 0$, the two points are linearly stable if $0 < \varepsilon < 3$ as the eigenvalues reduce to the following simple expressions:

$$\lambda_{\pm}^{F_2} = 1$$
$$\lambda_{\pm}^{F_1,F_3} = \pm\left(\frac{\varepsilon - 3}{\varepsilon}\right)^{1/2} . \qquad (10)$$

For $\varepsilon > 3$ F_1 and F_3 are stable choosing the negative sign and unstable choosing the positive sign.

We now study the dependence of the phase diagram and of the fixed points on the nonlinear parameter ε and on the damping coefficient γ. In this analysis, the numerical integration of Eq.(2) was performed according to the interpolating function object for the solution $y(\tau)$ as done in previous numerical calculations. First, we study the case with the positive linear term in Eq.(2). The phase diagram does not exhibit stable fixed points having real values so that in this case there are not fixed period of the oscillation apart from the trivial fixed point in the origin. In the phase diagram there is a continuous winding of the lines for small values of the damping parameter (γ =0.1) giving rise to an elliptical shape as shown in Fig.6. For larger damping (γ =0.5) the shape changes from a closed elliptical to an open spiral independently of the value of ε.

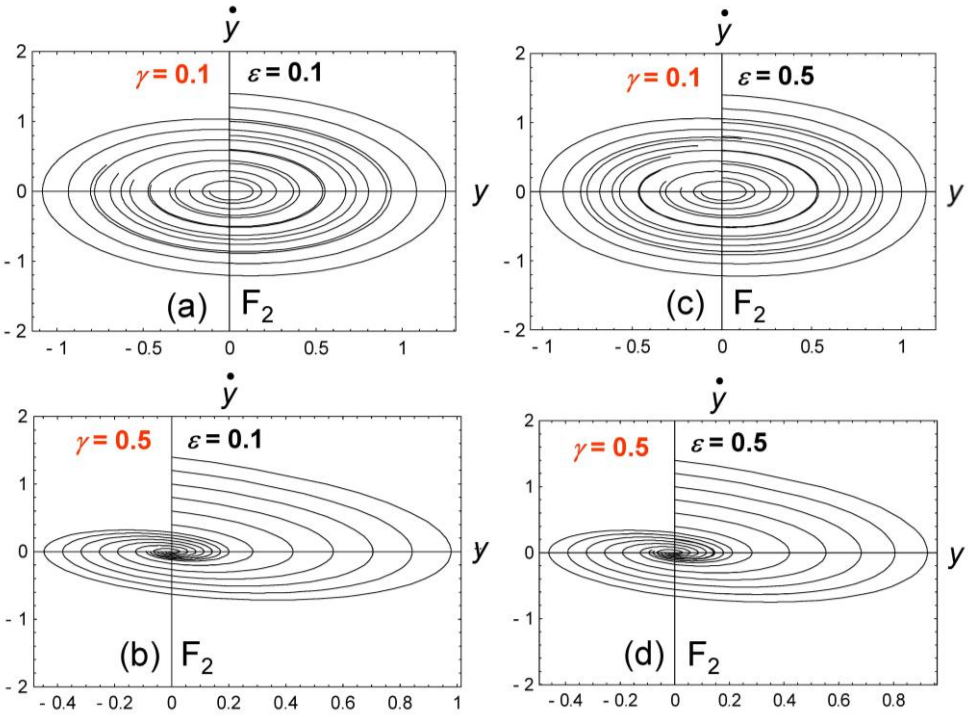

Fig. 6. Stability diagram with fixed point F_2 on the *x*-axis obtained from Eq.(2) with the positive sign in the linear term. (a): γ =0.1 and ε = 0.1. (b): γ =0.5 and ε = 0.1. (c): γ =0.1 and ε = 0.5. (d): γ =0.5 and ε = 0.5.

We now study the case with the negative linear term in Eq.(2). Even if this is a not a typical case in power systems it is instructive to discuss the dependence of the fixed points on the nonlinear parameter. For the values of the nonlinear parameter that ensure stability ($0 < \varepsilon < 3$) there is no continuous winding due to the presence of fixed periods of the oscillation as displayed in Fig.7. Fixed periods of the oscillation represented by the point F_1 and F_3 are symmetric with respect to the *y* axis, lie on the *x* axis and approach the origin with increasing ε. In particular, for $\varepsilon = 0.1$ $F_1 = (-3.16, 0)$ and $F_3 = (3.16,0)$, for $\varepsilon = 0.5$ $F_1 = (-1.41, 0)$ and $F_3 = (1.41, 0)$ as shown in Fig.7. For all the values of ε there is always a trivial fixed point $F_2 = (0,0)$. Note that the coordinates of the fixed points are independent of the values of the damping parameter. The corresponding eigenvalues are real for F_2, viz. $\lambda_+^{F_2} = 0.95$ and $\lambda_-^{F_2} = -1.05$ for every ε and for $\gamma = 0.1$ and $\lambda_+^{F_2} = 0.81$ and $\lambda_-^{F_2} = -1.31$ for $\gamma = 0.5$. Instead, as expected they are complex for F_1 and F_3, viz. $\lambda_\pm^{F_1,F_3} = -0.05 \pm j\,5.38$ for $\gamma = 0.1$ and $\lambda_\pm^{F_1,F_3} = -0.25 \pm j\,2.22$ for $\gamma = 0.5$. With no damping ($\gamma = 0$) the two eigenvalues become purely imaginary, namely $\lambda_\pm^{F_1,F_3} = \pm j\,5.39$ for $\varepsilon = 0.1$ and $\lambda_\pm^{F_1,F_3} = \pm j\,2.24$ for $\varepsilon = 0.5$.

The strongly deformed shape indicates non-linearity that is more evident in Fig.7(c) and (d). Interestingly, the lines become more stretched for $\varepsilon = 0.5$. Instead, for $\varepsilon = 0.1$ the shape is less deformed and this is an indication of the approach to the linear regime. At a fixed value of ε there is also an effect of the damping parameter on the lines topology. With increasing γ the winding of the lines reduces and the lines tend to assume the shape of open spirals around the two symmetric fixed points F_1 and F_3. This effect is more accentuated at $\varepsilon = 0.5$. With increasing the nonlinear parameter at fixed damping coefficient there are not qualitative changes of the lines topology. In the absence of damping the lines topology is very similar to that of Fig.7(a) and (b).

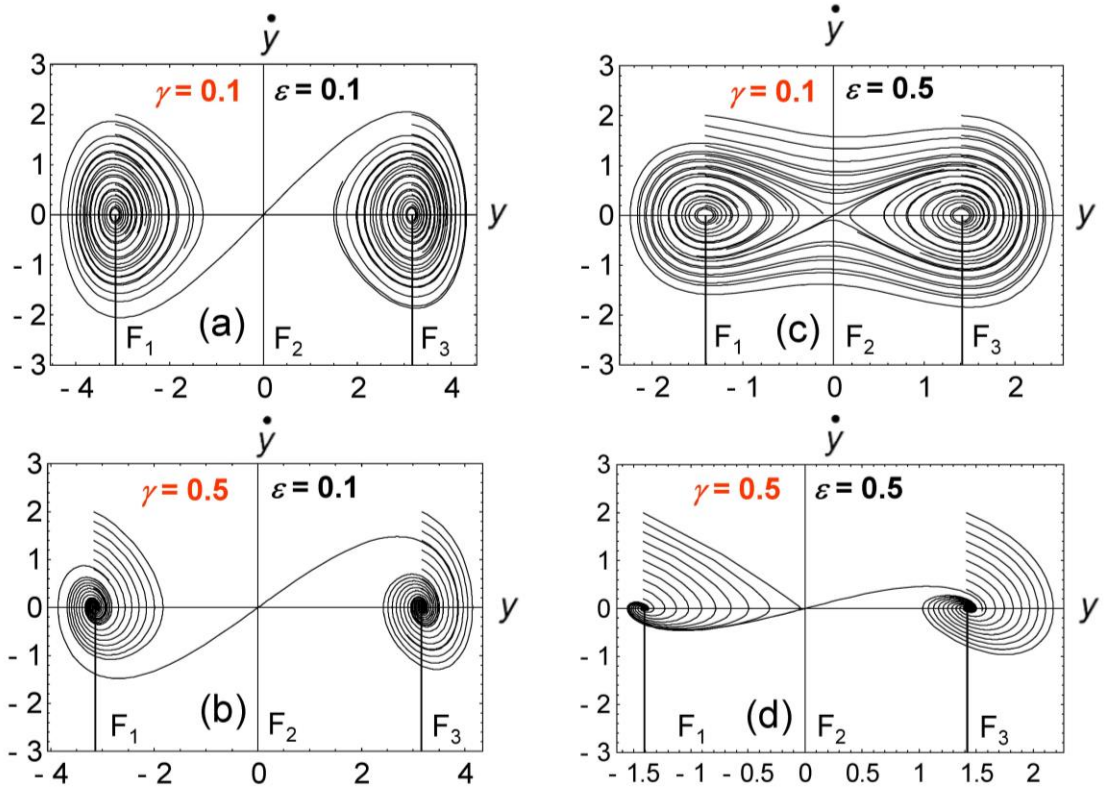

Fig. 7. Stability diagram with fixed points F_1, F_2 and F_3 on the *x*-axis obtained from Eq.(2) with the negative sign in the linear term. (a): γ =0.1 and ε = 0.1. (b): γ =0.5 and ε = 0.1. (c): γ =0.1 and ε = 0.5. (d): γ =0.5 and ε = 0.5.

In the next section a comparison between the numerical results obtained according to the proposed model and the behaviour of the measured $i(t)$ for different distribution lines is presented. This is done by assuming that $i(t)$ flowing in the distribution lines is a solution to the Duffing equation (cfr. Eq.(2)).

4. Results and discussion

In this section, the system under test is described in detail, and the behaviour of the measured current flowing in the circuit as a function of time is compared to the theoretical solution of the Duffing equation for several lines.

4.1. Description of the system under test

The system under test is a part of a SG constituted by several passive and active lines feeding both residential and commercial users. In particular, three lines were investigated, one active and two passive, having important load variations during the day and the week. The three-phase line L_1 is passive with a peak power of about 100 kW. The three-phase line L_2 is passive, it has a very low amount of PhotoVoltaic (PV) power (1 grid-connected PV plant, 6 kWp) and it has a peak absorbed power of 50 kW. The three-phase line L_3 is an active line with a great amount of PV power (over 100 kWp) and with a maximum peak of about 80 kW of absorbed power. Fig. 8 shows the L_3 line, the other two lines are similar. For every line investigated, we consider the current $i(t)$ flowing in a phase of the DL. Current measurements range between the end of September 2013 and the end of June 2014 for a total of 278 days, a period corresponding approximately to 9 months and covering three different seasons. In particular, the line L_1 has a great amount of residential users, the line L_2 has a prevalence of commercial users, and the line L_3 has several residential users fed also with grid-connected PV plants.

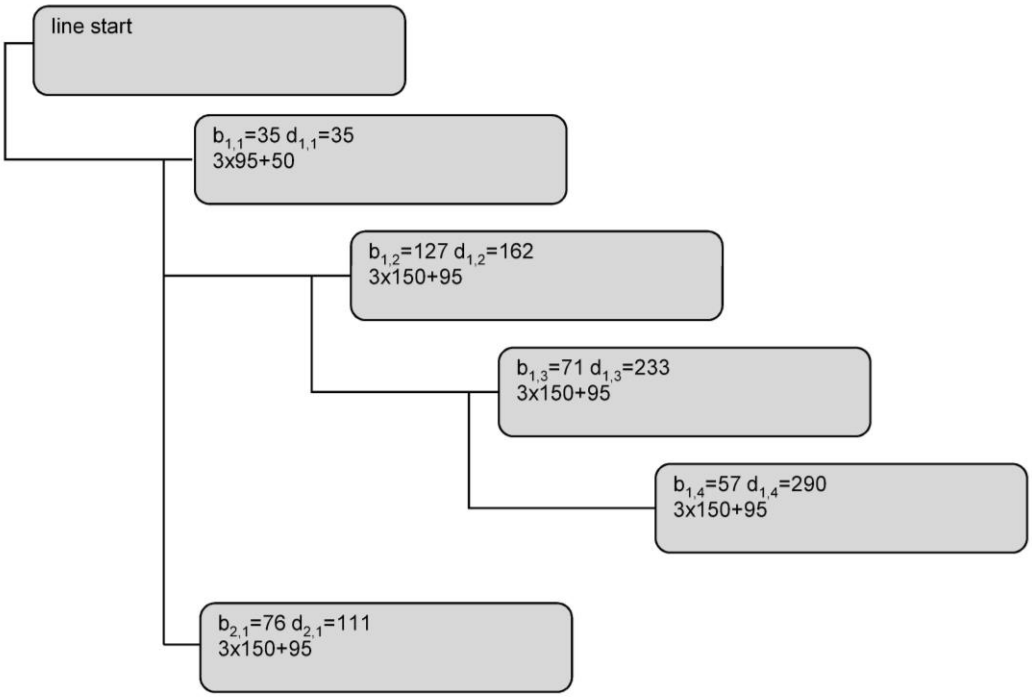

Fig. 8. Line L_3 of the system under study: $b_{j,k}$ is the length of the k-th branch of the j-th ramification, $d_{j,k} = b_{j,k}+d_{j,k-1}$ is the distance of the branch (j,k) from the line start. 3×150+95 stands for a tri-polar cable with section 150mm^2 and neutral conductor of 95 mm^2.

4.2. Measured current: time behaviour

The time behaviour of the current $i(t)$ in the whole sampling period for the three most representative lines L_1, L_2 and L_3 described in the previous subsection and for the a phase is shown in Fig.9 (a-c). The corresponding $i(t)$ for the central week of the sampling period are displayed in Fig.9(d-f). The deviation from a purely periodical behaviour is mainly related to the non-linearity effect as can be seen clearly in the temporal windows of one week where the profile of $i(t)$ is deformed with pointed crests and troughs.

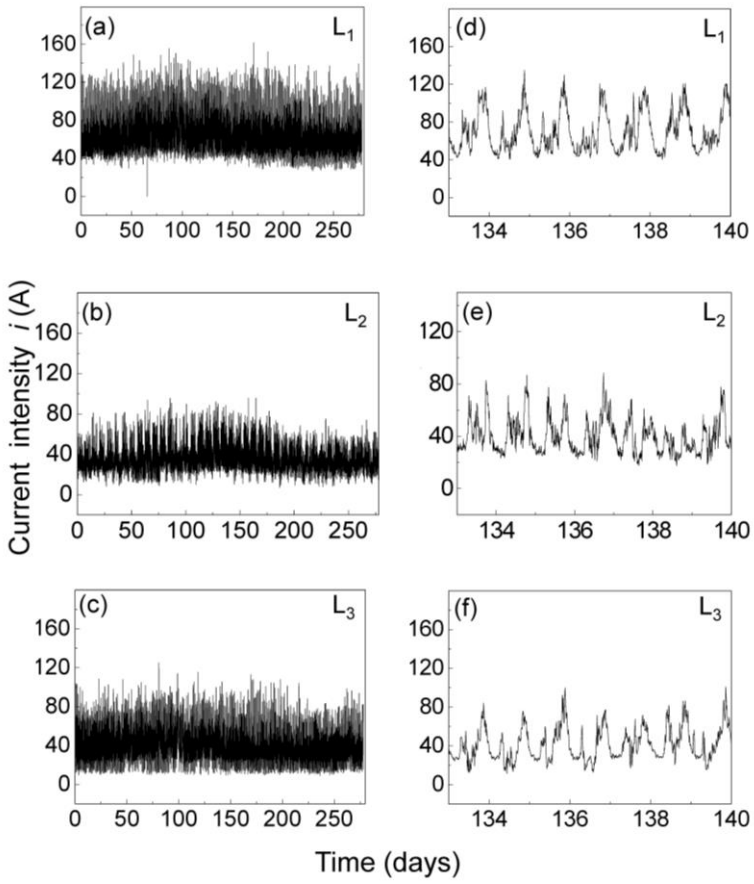

Fig. 9. Measured current vs. time. (a): $i(t)$ for the sampling period of the L_1 line. (b): as in (a), but for the L_2 line. (c): as in (a), but for the L_3 line. (d): $i(t)$ for a representative week of the L_1 line. (e):

as in (d), but for the L_2 line. (f): as in (d), but for the L_3 line.

Moreover, additional features of the current are: (a) the frequency and amplitude modulation; (b) the small damping effect with increasing t. Even though the signal is not purely periodic, it is possible to extract an approximate period T corresponding more or less to one day. Note that the $i(t)$ trend in the other weeks of the sampling period is very similar to the ones shown in Fig.9(d-f). Moreover, the time behaviour of the measured $i(t)$ for the other phases resembles the one displayed in Fig. 9.

A comparison between the measured current expressed in dimensionless units (normalized to the maximum intensity I_{max}) and the numerical solution to the Duffing equation (Eq.(2)) is shown in Fig.10 for the lines L_1, L_2 and L_3 during a one-week temporal window. The initial conditions $y(0)$ and $\dot{y}(0)$ for the solution to Eq.(2) are different for the three lines due to the different values assumed by the current and by its first derivative at $t = 0$. Also for the fitting procedure the numerical integration of Eq.(2) was performed by determining the function $y(\tau)$ via the interpolating function depending on the different initial conditions for the three lines. In the calculations the following representative values were used: $R = 5\ \Omega$, $L = 16$ mH, $C = 1\ \mu$F, $V_0 = 220$ V and $\omega = 314$ rad/s. The following dimensionless parameters appearing in Eq.(2) were found: $\gamma = R\sqrt{\frac{C}{L}} = 0.04$ and $\alpha = \frac{V_0\omega}{L}\frac{1}{I_{max}}\frac{1}{\omega_0^2} = \frac{0.07\ \text{A}}{I_{max}}$, where the maximum intensity I_{max} depends on the line analyzed. In particular, in the temporal window considered it is $I_{max} = 120$ A for L_1, $I_{max} = 88$ A for L_2 and $I_{max} = 100$ A for L_3.

The fitting procedure was performed by varying the value of the nonlinear parameter ε, which turned out be positive for every line studied. Hence, the associated behaviour of the measured current as a function of time is equivalent to that of a “hard spring” if compared to a mechanical system. The fitting procedure was also very sensitive to the initial conditions: $y(0) = -0.95$ and

$\dot{y}(0)=1$ for L_1, $y(0)$ = - 0.70 and $\dot{y}(0)=1$ for L_2, and $y(0)$ = -0.80 and $\dot{y}(0)=1$ for L_3. From the fitting procedure, by applying a least-square analysis it was found: $\varepsilon = 55 \pm 1$ for line L_1, $\varepsilon = 110 \pm 1$ for line L_2 and $\varepsilon = 80 \pm 1$ for line L_3 (Fig.10(a-c), respectively).

The comparison between the measured and the numerical current intensities is good especially regarding the amplitude and the periodicity of the signal. Nevertheless, the calculated current does not completely reproduce the double-peak profile typical of the measured signal. This discrepancy is not surprising. Indeed, it can be attributed to other effects that are not included in the present model based on the solution to the cubic Duffing equation. We have also found that this discrepancy is not due to the effect of additional quadratic or quintic terms or to the variation of other parameters governing the Duffing equation.

The time behaviour of the current of the L_2 line having a prevalence of commercial users has the largest deviation from the linearity, which in turn leads to a deviation from a purely periodical trend. However, to a lesser extent, non-linear effects characterize also the current of the lines L_1 and L_3.

In order to have a further confirmation about the main role played by the non-linearity parameter ε in determining the time behaviour of the $i(t)$ signal, also the damping coefficient $\gamma = 0.04$ fixed by the typical parameters of the circuit was varied in the realistic range $0.03 \div 0.05$. This was done in addition to the variation of ε by assuming small variations of R, L and C. It has been found that the effect of γ on the trend of the current intensity is negligible for the considered range of values confirming the above listed values of ε for the three lines. This analysis confirms that the main influence on the time behaviour of the current intensity is given by non-linear effects for every line considered.

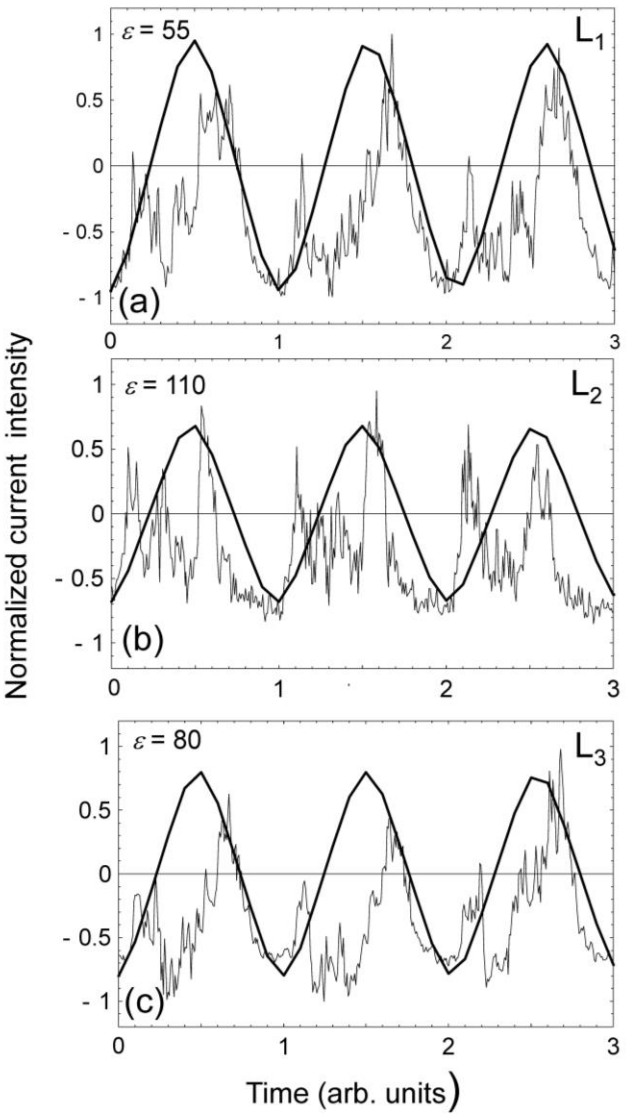

Fig. 10. Thick line: Current vs. time calculated according to Eq.(2). Thin line: measured current. (a): L_1 line. (b): L_2 line. (c): L_3 line. The value of the fitted non-linear parameter is indicated.

5. Conclusion

In summary, in this paper it has been studied the time behaviour of an electrical signal by solving the cubic Duffing equation both analytically and numerically. The analysis has been carried out for different values of the nonlinear, damping and forcing parameters. An exact analytical solution has been obtained for the special case of free generators and negligible damping, expressed in terms of a Jacobian elliptic function.

In addition, a stability analysis of the cubic Duffing equation has been carried out for different values of the nonlinear parameters and the fixed points have been determined for both positive and

negative value of the linear parameter. The value of the nonlinear parameter has been accurately fitted by comparing the theoretical solution to the Duffing equation with the measured current data of DLs belonging to a SG. From the fitting procedure, it was found that the behaviour of the current is nonlinear and equivalent to the one of a “hard spring” as should be expected for an electrical signal flowing in DLs. In particular, the DL having a large number of commercial users exhibits the greatest deviation from the linearity. However, nonlinear effects are present also in the other DLs having a predominance of residential users.

Finally, as resulting from our fitting procedure applied to a real electrical signal, the developed model based on the Duffing oscillator permits to describe the behaviour of a real distribution line depending from the typology of the connected users (either commercial or residential). In fact, the nonlinear parameters of the Duffing oscillator can be used as indicators of the nonlinearity degree of the electrical signal. This information is particularly important for the distribution system operator during the management of the electrical grid.

Acknowledgement

The paper has been written within the framework of the project “RES NOVAE - Reti, Edifici, Strade - Nuovi Obiettivi Virtuosi per l’Ambiente e l’Energia”. This project is supported by the Italian University and Research National Ministry (MIUR) and competitiveness program that Italy is developing to promote “Smart Cities Communities and Social Innovation”.

References

[1] P. Holmes, Ninety plus thirty years of nonlinear dynamics: less is more and more is different, Int. J. Bifurcat. Chaos 15 (2005) 2703-2716.

[2] S.W. Shaw, B. Balachandran, A review of nonlinear dynamics of mechanical systems in year 2008, JSDD 2 (2008) 611–640.

[3] R. Lifshitz, M.C. Cross, Nonlinear dynamics of nanomechanical and micromechanical resonators. Reviews of Nonlinear Dynamics and Complexity, vol. 1, John Wiley, 2008.

[4] J. Guckenheimer and P. Holmes, Nonlinear Oscillations, Dynamical Systems, and Bifurcations of Vector Fields, Springer, New York, 1983.

[5] F.C. Moon, Chaotic Vibrations, Wiley, New York, 1987.

[6] J.K. Hale, Oscillations in Nonlinear Systems, McGraw-Hill, New York, 1963.

[7] A.M. Kosevich, B.A. Ivanov, and A.S. Kovalev, Magnetic Solitons, Phys. Rep. 194 (1990) 117-238.

[8] J. Rasmussen and K. Rypdal, Blow-up in nonlinear Schroedinger equations-I A general review, Phys. Scr. 33 (1986) 481-497.

[9] R. Zivieri, G. Santoro, V. Bortolani, Anharmonicity on Al (100) and Al (111) surfaces, Phys. Rev. B 59 (1999) 15959-15965.

[10] The Duffing equation: Nonlinear oscillators and their behaviour, I. Kovacic, M. J. Brennan eds., John Wiley & Sons, Ltd., 2011.

[11] Y. Ueda, Randomly transitional phenomena in the system governed by Duffing's equation, J. Stat. Phys. 20 (1979) 181–196.

[12] Y. Ueda, Steady Motions Exhibited by Duffing's Equation: A Picture Book of Regular and Chaotic Motions, in Hao Bai-Lin, D. H. Feng, and J.-M. Yuan, (eds.), New Approaches to Nonlinear Problems. SIAM, Philadelphia, 1980.

[13] A. Elías-Zúñiga, Exact solution of the cubic-quintic Duffing oscillator, Appl. Math. Model. 37 (2013) 2574-2579.

[14] A. Elías-Zúñiga, Solution of the damped cubic-quintic Duffing oscillator by using Jacobi elliptic functions. Appl. Math. Comput. 246 (2014) 474-481.

[15] E. Yusufoğlu (Agadjanov), Numerical solution of Duffing equation by the Laplace decomposition algorithm, Appl. Math. Comput. 177 (2006) 572–580.

[16] F. Geng, Numerical solutions of Duffing equations involving both integral and non integral forcing terms, Comput. Math. Appl. 61 (2011) 1935–1938.

[17] S. K. Lai, C. W. Lim, B. S. Wu, C. Wang, C. Q. Zeng, X. F. He, Newton-harmonic balancing approach for accurate solutions to nonlinear cubic-quintic Duffing oscillators, Appl. Math. Model. 33 (2009) 852-866.

[18] D. E. Panayotounakos, E. E. Theotokoglou, M. P. Markakis, Exact analytic solutions for the damped Duffing nonlinear oscillator, C. R. Mecanique 334 (2006) 311-316.

[19] S. Nourazar, A. Mirzabeigy, Approximate solution for nonlinear Duffing oscillator with damping effect using the modified differential transform method, Sci. Iran. B 20 (2013) 364-368.

[20] G.-A. Zakeri, E. Yomba, Exact solutions of a generalized autonomous Duffing-type equation, Appl. Math. Model. 39 (2015) 4607-4616.

[21] D. D'Humieres, M.R. Beasley, B.A. Huberman, A. Libchaber, Chaotic states and routes to chaos in the forced pendulum, Phys. Rev. A 26 (1982) 3483–3496.

[22] A.H. Nayfeh, N.E. Sanchez, Bifurcations in a forced softening Duffing oscillator, Int. J. Nonlinear Mech. 24 (1989) 483–497.

[23] M.S. Soliman, J.M.T. Thompson, Integrity measures quantifying the erosion of smooth and fractal basins of attraction, J. Sound Vib. 135 (1989) 453–475.

[24] U. Parlitz, Common dynamical features of periodically driven strictly dissipative oscillators, Int. J. Bifurcat. Chaos 3 (1993) 703–715.

[25] U. Parlitz, W. Lauterborn, Superstructure in the bifurcation set of the Duffing equation, Phys. Lett. A 107 (1985) 351–355.

[26] H. Vahedi, G.B. Gharehpetian, M. Karrari, Application of Duffing oscillators for passive islanding detection of inverter-based distributed generation units, IEEE Trans. Power Del. 27 (2012) 1973-1983.

[27] G. Wang, S. He, A quantitative study on detection and estimation of weak signals by using chaotic duffing oscillators, IEEE Trans. Circuits Syst. I, Fundam. Theory Appl. 50 (2003) 945–953.

[28] A. Agarwal, J. H. Lang, Foundations of analog and digital electronic circuits, Morgan Kaufmann, San Francisco, 2005.

[29] H. Mostafa, M. Anis, M. Elmasry, Negative capacitance circuits for process variations compensation and timing yield improvement, IEEE International Conference on Electronics, Circuits, and Systems (ICECS'13), Abu Dhabi, United Arab Emirates, IEEE, pp. 277-280, (2013).

Figure captions

Fig. 1. Analytical solution to the DDE as a function of time for different values of the nonlinear parameter and for $\gamma = 0$ and $\alpha = 0$. (a): $\varepsilon = 0.1$. (b): $\varepsilon = 1$. (c): $\varepsilon = 2$. (d): $\varepsilon = 10$. (e): $\varepsilon = 100$. (f): $\varepsilon = 1000$.

Fig. 2. Solution to the DDE at fixed damping coefficient $\gamma = 0.5$ and with no forcing term ($\alpha = 0$) for different values of the nonlinear parameter. (a): $\varepsilon = 1$. (b): $\varepsilon = 10$. (c): $\varepsilon = 100$.

Fig. 3. Solution to the DDE at fixed damping coefficient $\gamma = 0.5$ for different values of the forcing term and of the nonlinear parameter. (a): $\varepsilon = 1$, $\alpha = 1$. (b): $\varepsilon = 10$, $\alpha = 1$. (c): $\varepsilon = 100$, $\alpha = 1$. (d): $\varepsilon = 1$, $\alpha = 10$. (e): $\varepsilon = 10$, $\alpha = 10$. (f): $\varepsilon = 100$, $\alpha = 10$. In all case the angular frequency of the forcing term is $\tilde{\omega} = 1$.

Fig. 4. Solution to the DDE at fixed damping coefficient $\gamma = 0.5$, fixed positive nonlinear parameter $\varepsilon = 1$, two different values of the forcing term α as a function of the forcing frequency $\tilde{\omega}$. (a): $\tilde{\omega} = 1$ and forcing term $\alpha = 1$. (b): $\tilde{\omega} = 2$ and forcing term $\alpha = 1$. (c): $\tilde{\omega} = 10$ and forcing term $\alpha = 1$. (d): $\tilde{\omega} = 1$ and forcing term $\alpha = 10$. (e): $\tilde{\omega} = 2$ and forcing term $\alpha = 10$. (f): $\tilde{\omega} = 10$ and forcing term $\alpha = 10$.

Fig. 5. Solution to the DDE at fixed damping coefficient γ = 0.5 and α =1 as a function of the negative nonlinear parameter. (a): ε = -0.1. (b): ε = -0.4. (c): ε = -0.5. (d): ε = -0.6.

Fig. 6. Stability diagram with fixed point F_2 on the *x*-axis from Eq.(2) with the positive sign in the linear term. (a): γ =0.1 and ε = 0.1. (b): γ =0.5 and ε = 0.1. (c): γ =0.1 and ε = 0.5. (d): γ =0.5 and ε = 0.5.

Fig. 7. Stability diagram with fixed points F_1, F_2 and F_3 on the *x*-axis from Eq.(2) with the negative sign in the linear term. (a): γ =0.1 and ε = 0.1. (b): γ =0.5 and ε = 0.1. (c): γ =0.1 and ε = 0.5. (d): γ =0.5 and ε = 0.5.

Fig.8. Line L_3 of the system under study: $b_{j,k}$ is the length of the *k-th* branch of the *j-th* ramification, $d_{j,k} = b_{j,k}+d_{j,k-1}$ is the distance of the branch (j,k) from the line start. 3x150+95 stands for a tri-polar cable with section 150mm^2 and neutral conductor of 95 mm^2.

Fig. 9. Measured current vs. time. (a): i(t) for the sampling period of the L_1 line. (b): as in (a), but for the L_2 line. (c): as in (a), but for the L_3 line. (d): *i*(*t*) for a representative week of the L_1 line. (e): as in (d), but for the L_2 line. (f): as in (d), but for the L_3 line.

Fig. 10. Thick line: Current vs. time calculated according to Eq.(2). Thin line: measured current. (a): L_1 line. (b): L_2 line. (c): L_3 line. The value of the fitted non-linear parameter is indicated.